Observation of Monoenergetic Electrons from Two-Pulse Ionization Injection in Quasilinear Laser Wakefields

M. W. von der Leyen,[1,3,*] J. Holloway,[1] Y. Ma,[2] P. T. Campbell,[2] R. Aboushelbaya,[1] Q. Qian,[2] A. F. Antoine,[2] M. Balcazar,[2] J. Cardarelli,[2] Q. Feng,[1] R. Fitzgarrald,[2] B. X. Hou,[2] G. Kalinchenko,[2] J. Latham,[2] A. M. Maksimchuk,[2] A. McKelvey,[2] J. Nees,[2] I. Ouatu,[1] R. W. Paddock,[1] B. Spiers,[1] A. G. R. Thomas,[2] R. Timmis,[1] K. Krushelnick,[2] and P. A. Norreys[1,3,4]

[1]*Department of Physics, University of Oxford, Oxford OX1 3PU, United Kingdom*
[2]*Center for Ultrafast Optical Science, University of Michigan, Ann Arbor, Michigan 48109, USA*
[3]*John Adams Institute for Accelerator Science, Denys Wilkinson Building, Oxford OX1 3RH, United Kingdom*
[4]*Central Laser Facility, STFC, Rutherford Appleton Laboratory, Didcot, OX11 0QX, United Kingdom*

(Received 9 November 2021; revised 31 January 2023; accepted 9 February 2023; published 10 March 2023)

The generation of low emittance electron beams from laser-driven wakefields is crucial for the development of compact x-ray sources. Here, we show new results for the injection and acceleration of quasimonoenergetic electron beams in low amplitude wakefields experimentally and using simulations. This is achieved by using two laser pulses decoupling the wakefield generation from the electron trapping via ionization injection. The injection duration, which affects the beam charge and energy spread, is found to be tunable by adjusting the relative pulse delay. By changing the polarization of the injector pulse, reducing the ionization volume, the electron spectra of the accelerated electron bunches are improved.

DOI: 10.1103/PhysRevLett.130.105002

Laser-driven wakefield accelerators accelerate electrons in the electrostatic field of an electron plasma wave driven by an ultrashort laser pulse. The longitudinal electric fields in the plasma structure ("wakefield") can be orders of magnitude higher than in conventional radio frequency particle accelerators, paving the way for ultracompact and cost-effective electron sources. The generated electron beams find direct applications in radiotherapy [1,2] or indirect applications through driving soft [3] or hard [4–6] x rays for imaging purposes. The great potential of these devices has driven promising research in the field of plasma wakefield acceleration since its inception in 1979 [7]. Following breakthrough experiments in 2004 [8–10], laser-driven wakefields have since then achieved electron beams with peak energies of 8 GeV [11]. To increase the maximum achievable beam energy, operation at lower electron density values is favorable ($W_{\max} \propto n_e^{-1}$ [12]). However, this means that, due to the lower field strength ($E_0 \propto n_e^{1/2}$ [13]), the distance over which particles are accelerated has to be large. This implies laser diffraction becomes a substantial problem. A promising mitigation technique for laser diffraction is the guiding of laser pulses of weakly relativistic intensity in a preformed plasma channel [14–19].

In the nonlinear wakefield regime (normalized laser amplitude $a_0 > 1$), the ponderomotive force of the intense laser pulse generates electric fields of large amplitude and an increased overlap between accelerating and focusing fields compared to the quasilinear regime ($a_0 < 1$). However, the latter is compatible with intensity-independent guiding techniques for laser pulses. In both cases, electrons have to be trapped in the wakefield to be accelerated. In the strongly nonlinear case the wave breaks, injecting electrons into the wakefield—this process is difficult to control and leads to large energy spread and beam emittance (measure of the spread of particles' transverse position and momentum values). Furthermore, the effect of laser self-focusing [20] can cause injection of multiple electron beams every time the threshold is reached. Other mechanisms such as modified density profile injection [21–25] and ionization injection [26–29] have shown promising results in nonlinear wakefield accelerators. All of these mechanisms try to minimize the injection duration in order to achieve low beam energy spread and emittance. Since electron injection via wave breaking, density profile modifications, or direct ionization are not achievable in the quasilinear regime, electrons must be injected by a different mechanism.

Faure *et al.* [30] showed that colliding beams could create high-quality beams, albeit in a counterpropagating geometry that rules out the use of plasma channels.

Hidding *et al.* [31] proposed to use laser pulses propagating in a beam-driven wakefield bubble to inject electrons into the wakefield without changing the wakefield structure. Shortly after, Bourgeois, Cowley, and Hooker [32] proposed to inject electrons in a laser-driven wakefield accelerator setting using a quickly diffracting injector pulse propagating one plasma wavelength behind the (slowly diffracting) driver pulse in hydrogen doped with nitrogen. Close to focus, the injector briefly increases the wakefield amplitude while ionizing nitrogen atoms' sixth and seventh electrons ($e_{\mathrm{N}}^{6,7}$), which are trapped in the wakefield. Then, the injector diffracts below the ionization threshold and the wakefield adiabatically evolves into a quasilinear state in which electrons are further accelerated. Here, the beam emittance and energy spread depend on careful optimization of experimental parameters such as focal spot size, intensity, relative spatial and temporal position between the pulses, and beam quality. Thomas *et al.* [33] studied the propagation of two beams of different diffraction length at a set delay and found partial guiding of the trailing pulse.

Here, we show the first experimental demonstration of a copropagating two-pulse ionization injection mechanism. We demonstrate that injection is possible over a pulse delay region on the order of the plasma wavelength $\lambda_p \equiv 2\pi c\sqrt{m_e\epsilon_0/(n_e e^2)}$ (ϵ_0 is the vacuum permittivity) and that the beam charge and energy spread of accelerated electrons depend on the injector pulse polarization (which was observed to have significant impact on electron trajectories in the ionization injection process [34]).

The experiment was conducted using the HERCULES laser (University of Michigan) delivering pulses of 9 J in 39 fs (FWHM). The main beam was split in the vacuum chamber using a 2-in. pickoff mirror. The inner part (drive pulse) was focused using an $f/40$ parabola and the outer annular part (injector pulse), after being optimized using adaptive optics, was focused using an $f/3.8$ off-axis parabola that had a central hole of 1.5 cm diameter. This allowed the drive beam to pass through the optic parallel to the injector. Delay stages changed the arrival time of either pulse thus giving control over the relative longitudinal pulse separation Δt. The measured peak amplitudes of the pulses were $a_{0,\mathrm{drive}} = 0.75$ and $a_{0,\mathrm{inject}} = 2.46$ ($a_{0,\mathrm{drive}} = 0.71$ and $a_{0,\mathrm{inject}} = 1.88$ when evaluating the peak from a fitted Gaussian using the beam waist and energy as input rather than local peak values in the intensity distribution). A schematic of the setup is shown in Fig. 1. The electron density was measured using an interferometry probe. To find the optimal pulse separation, spatial interference fringes (whose magnitudes depend on the degree of pulse overlap) were observed using a focal spot camera. After strongest overlap was found and used as a reference value (accurate to ± 10 μm), the pulse separation was measured from the delay stage actuator readings (smallest increment 2 μm). Electron beam energies were measured using two rare earth intensifying ("Lanex") screens placed behind the

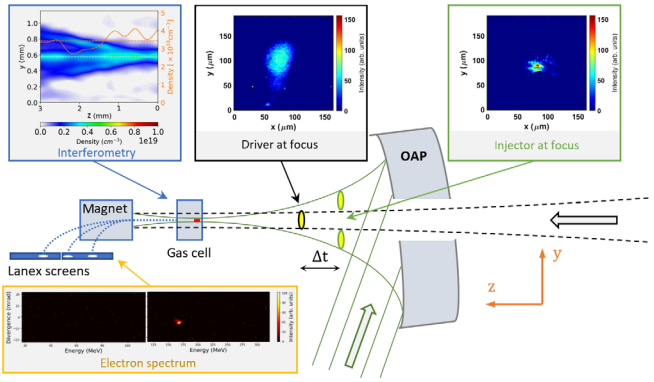

FIG. 1. Schematic of the experimental setup in the target chamber. The drive beam path is depicted as a dashed black line. The annular injector beam path is depicted as a green line. Both pulses travel through the gas cell from the right-hand side to the left-hand side. The red area in the gas cell indicates the volume of injection. The blue dashed lines represent possible electron trajectories.

interaction region. Using a 1.03 T magnet, electron beams were deflected onto the screens. The location of the intersection of electron trajectory and screen depends on the particle energy and divergence angle. To find the particle energy, a calibration simulation of the spectrometer was conducted using a three-dimensional relativistic Boris pusher [35,36].

In our experiment, the delay between the two pulses was scanned. The first run used a gas mixture of 97% helium and 3% nitrogen with both pulses having linear and parallel polarization. The average peak density measured using an interferometry probe was 4.32×10^{18} cm^{-3} ($\pm 5.8\%$) corresponding to a plasma wavelength of $\lambda_p = 16.1$ μm. First, several test shots were taken with either laser pulse blocked in which no accelerated electron beams were detected. This ensured neither pulse was able to self-inject electrons. Then, the pulse delay between the unblocked pulses was scanned over a distance of 52 μm starting 18 μm (± 10 μm) from beam overlap (injector in front) and delaying the injector from this position. Figure 2 presents an analysis of all shots taken in this run. The values were obtained after integrating the emitted intensity from the Lanex screens over the divergence angle, subtracting the background noise from a reference shot, and using a moving average to smooth high-frequency oscillations caused by hot pixels. It is found that electrons are only accelerated in a narrow pulse delay range $\delta = 12$ μm with a mean delay of $\overline{\Delta z} = 10.2$ μm. The spectra show two different electron beam characteristics: single-bunch and double-bunch beams (two peaks of different energy indicating injection of electrons into two different wakes). In Run II [average electron density $\bar{n}_{e,\mathrm{peak}} = 4.45 \times 10^{18}$ cm^{-3} ($\pm 9.3\%$)], a circularly polarized injector was used (quarter wave plate rotated with energy kept constant and negligible impact on the focus). Except one, all accelerated beams were

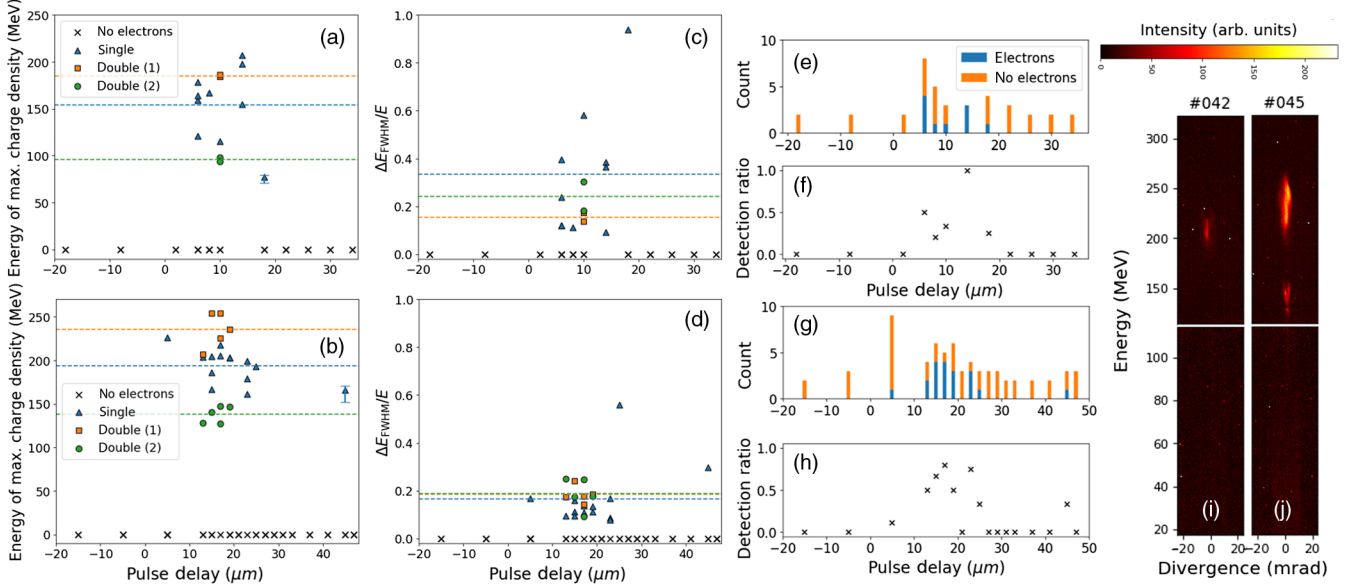

FIG. 2. Data obtained from the Lanex screens measuring the electron spectrum (top, linearly polarized injector pulse; bottom, circularly polarized injector pulse). Panels (a) and (b) show the energy values of the electron charge density peak(s) plotted against the relative delay between pulses. Positive values correspond to a trailing injector pulse. The dashed lines show the mean value of each electron bunch type. For clarity, error bars corresponding to the calibration curve are not shown except for one sample shot. The maximum uncertainty values are −8.1% and +2.8%. Panels (c) and (d) show the corresponding maximal FWHM energy spread plotted against pulse delay. Panels (e) and (g) show the number of successful and unsuccessful shots at each delay value. Panels (f) and (h) present the ratio of successful shots over the total number of shots at each delay position. Panels (i) and (j) show typical spectra of single (i) and double (j) bunches as observed on the two Lanex screens from shots using a circularly polarized injector pulse (Run II). These two shots were taken at a delay of $\Delta z = 19$ μm.

observed over a pulse delay range of $\delta = 20$ μm with a mean delay of $\overline{\Delta z} = 17.2$ μm. Compared to Run I, the average electron beam peak energy is increased and the FWHM energy spread is decreased indicating a smaller injection area and/or shorter injection duration. This stems from the reduced peak intensity of circularly polarized pulses. The electric field in linearly polarized pulses is $\boldsymbol{E} = E_0 \cos(kz - \omega t)\hat{\boldsymbol{e}}_x$ and goes through zero in contrast to light of circular polarization where $\boldsymbol{E} = (1/\sqrt{2})E_0(\cos(kz-\omega t)\hat{\boldsymbol{e}}_x + \sin(kz-\omega t)\hat{\boldsymbol{e}}_y)$. To reach equal average intensity, the instantaneous peak intensity must necessarily be larger for linearly polarized light, which leads to a larger injection volume. Again, both electron beam types were observed where the double bunch was observed over a broader region of laser pulse delay. The ratio between the energy peaks of the second and first bunch is consistent at 0.60 (±0.03) indicating trapping in consecutive wakefield buckets at consistent phase positions.

We also measured the relative spatial jitter (assuming fixed injector position due to short focal length of the off-axis parabola; larger optics are typically more strongly affected by vibrations). The transverse focal spot position was measured from a re-imaged and calibrated focal spot using light leaking through a mirror in the beamline before the final focusing parabola. Between $\Delta z = 5$ μm and 25 μm, the transverse focal spot position center of mass of unsuccessful shots (no beam observed) is shifted with respect to that of successful shots by 11.8 μrad in y direction and 2.5 μrad in x direction. This means that with decreased jitter, the injection probability is expected to be higher. Electrons are injected up to a focal spot separation of $\sim \pm 40$ μm (comparable to driver spot size but significantly larger than injector spot size) in the x-y plane showing certain robustness for the present laser parameters. The injector is able to inject particles into the offset wakefield while converging or diffracting. This is possible because of the large effective focal spot area with enough power to inject electrons in the wings of the pulse. Because of the annular shape of the beam, the ring of maximum intensity preserves higher intensity off-axis compared to a Gaussian beam [37] enabling injection behind the focus into an offset wakefield. We also found that fluctuations in electron density (between 3.8 and 5.3×10^{18} cm^{-3}) do not impact the injection probability, supporting the argument of dual-pulse injection and demonstrating its stability.

The electron beam divergence in Run II was less than 10 mrad for all shots. The difference to typical electron beams of broad spectrum from wave breaking (see Refs. [34,38–40]) is evident in panels (i) and (j) of Fig. 2.

Changing to pure helium (Run III) produced no electron beams at any pulse delay implying that ionization of $e_N^{6,7}$ is indeed the reason for injection. Changing to 95% helium/5% nitrogen (Run IV) increased ΔE to previous runs,

decreased the pulse delay injection region, and increased the likelihood of injection within this narrow region. All shots displaying accelerated electrons are found in a region of $\delta = 10$ μm and 88% within $\delta = 6$ μm (between pulse delay values of $\Delta z = 16$ μm and 22 μm). In this region, only two shots did not show electron signals.

This suggests injection by the injector and acceleration of the injected beam in the driver wakefield showing that the benefits of both—long driving distance and short injection time—can be leveraged. Ideally, a reduced injector focal spot and lower pulse intensities are used to reduce the emittance (proportional to the electron displacement from the central axis).

We also conducted 2D particle-in-cell simulations using EPOCH [41]. The annular injector was simulated using two pulses crossing at an angle of $\alpha = 6.2°$, which is chosen to match the angle at which the experimentally measured annular beam's maximum intensity peaks diverge. In order to keep both pulses' intensities below the self-injection threshold (which is decreased in the ideal simulation environment of perfect beamlet overlap—which is not necessarily given in the experiment—and, in addition, differs between 2D (simulation) and 3D (experiment) geometries) at the experimentally found electron density of $n_e = 4.45 \times 10^{18}$ cm^{-3} (helium doped with 3% nitrogen), we used reduced values of $a_{0,\mathrm{drive}} = 0.63$ and $a_{0,\mathrm{inject}} = 2.16$. The simulations used 30 cells per laser wavelength longitudinally and 6.24 cells per laser wavelength transversally spanning an area equivalent to 70 μm × 770.67 μm. The beam polarization was linear in the simulation plane. To avoid unphysical injection at a sharp density step, a 100 μm ramp was implemented. All pulses focus at $z = 300$ μm. The pulses propagated for 4 mm. We used open boundary conditions.

There could be two reasons for this. The first one is the uncertainty of the pulse delay measurement in the experiment. Given that the delay is rather persistent in both experimental runs, however, we think that it is more likely related to the sensitivity of the process on the simulation parameters—consequently a simulation is unlikely to reproduce the exact experimental conditions.

A parameter scan over pulse separation was performed. Figure 3 shows the trapped electron density and the kinetic energy in the simulation box for various pulse delays after 13.3 ps. Electrons are trapped over a larger pulse delay range than in [32]. For strong pulse overlap more charge is injected into the wakefield buckets. While perfect beam overlap (temporally) is within the uncertainty of the experimental measurement and could indeed be the delay at which the injection process occurs, the consistency in both runs toward a larger pulse separation indicates that the simulation does not account for all physical aspects due to the effect's sensitivity on beam and plasma parameters (while at a delay of 1 plasma wavelength the transverse beam overlap may not be the deciding feature for injection,

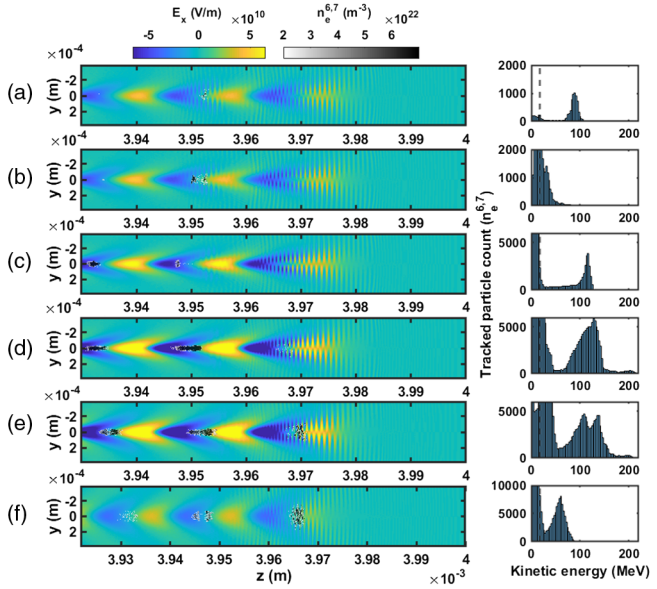

FIG. 3. Results from two-dimensional particle-in-cell simulations. Left: Longitudinal electric field strength and electron density from the sixth and seventh nitrogen ionization levels (above $n_e = 2 \times 10^{22}$ m^{-2}). Right: Kinetic energy associated with the same electrons. The separation in z between the pulses is λ_p (15.8 μm) (a), 0.75 λ_p (11.9 μm) (b), 0.5 λ_p (7.9 μm) (c), 0.25 λ_p (4.0 μm) (d), 0 (e), and −0.5 λ_p (−7.9 μm) (f) where positive values indicate that the drive pulse is ahead.

it may well be the case at perfect overlap where both pulses' electromagnetic fields combine to inject electrons). In the simulation, injection stops at a delay of ≤ 1.5 λ_p (delay was scanned in steps of 0.25 λ_p). In the experiment, injection probability falls off steeply if the delay increases beyond $\sim\lambda_p$ (linear polarization) or ~ 1.5 λ_p (circular polarization) with only one detected shot beyond this region. The peak electron energy in the simulations was found at $E_{\mathrm{max,peak}} =$ 138.4 MeV (leading high charge peak) and 198.7 MeV (low charge peak) at perfect overlap. In the experiment using linear polarization, the average peak energy was $E_{\mathrm{avg,peak}} = 159.3$ MeV with a maximum of $E_{\mathrm{max,peak}} =$ 206.9 MeV at a pulse delay of 0.87 λ_p. The narrowest energy spread in the simulation was 9% at a pulse delay of λ_p. In the experiment, the same value was found but at a pulse delay of 0.87 λ_p. At perfect overlap, a pulse shape with two energy peaks is observed—experimentally (linear polarization), this behavior was only observed at 10 μm. Yet, experimental results are impacted by shot-to-shot fluctuations in transversal beam overlap, average electron density, and local electron density from partial self-focusing of wavefront parts, which may cause the results to deviate.

The maximum (drive) pulse amplitude in the simulations at the final time step ranges between $a_0 = 0.75$ (f) and 1.23 (d) showing that a focusing effect is present. The total on-axis intensity is increased while the quick diffraction of

the injector pulse keeps the effective intensity below the ionization injection threshold behind the focus. Partial guiding of a strongly diffracting pulse copropagating in the correct phase with a weakly diffracting pulse that acts as the guide pulse has been shown in [33] where monoenergetic electrons between 10 and 30 MeV were produced in the interaction with a high-density gas jet. Note that ionization injection was not present in the mentioned article.

Additional simulations (not shown in Fig. 3) confirmed the presence of electron injection at y separation of up to ± 40 μm. As expected, the amount of charge accelerated and the peak energy are inversely proportional to the separation distance due to the reduced intensity at the point of injection (behind the focus) and the reduced acceleration length from the point of injection.

While the simulations in Bourgeois *et al.* suggest a relative energy spread as low as 2%, the electron beams found in this Letter have a lower limit of 7%. The normalized emittance found by Bourgeois *et al.* was $\epsilon_{\mathrm{n,rms}} = 5$ μm at minimal relative energy spread. While not measured experimentally, a similar value of $\epsilon_{\mathrm{n,rms}} = 3.7$ μm was found from our simulations considering electrons in the first wakefield bucket. Pollock *et al.* [29] showed that their broad spectrum beam from ionization injection can be optimized using a second accelerator stage to achieve relative energy spreads of less than 5%. McGuffey *et al.* [26] (using high electron densities of $>1 \times 10^{19}$ cm^{-3}) and Mo *et al.* [28] (using a highly nonlinear wakefield) find electron beams with peaks of several percent energy spread. In contrast to these articles, however, the 2PII mechanism is compatible for use with a linear wakefield driver in a low-density channel.

The work presented in this Letter has shown that quasimonoenergetic electrons can be injected into a quasilinear wakefield using a short Rayleigh-range injector pulse. This method can be optimized by tuning the injector pulse's intensity, optimizing its focal spot and wavefront properties, and minimizing the drive pulse's spatial jitter. The observed method is compatible with beam guiding using preformed channels and can therefore be used to generate high-energy electron beams. Furthermore, to increase the wall-plug efficiency, a multipulse driver [42] can be used that is also compatible with the presented injection mechanism.

The authors acknowledge R. Shalloo and A. Picksley for useful discussions on density analysis. This work has been funded by UKRI-STFC Grants No. ST/P002048/1 and No. ST/V001655/1 along with UKRI-EPSRC Grants No. EP/R029148/1 and No. EP/L000237/1. The authors gratefully acknowledge support from the U.S. Department of Energy's Office of Fusion Energy Sciences' LaserNetUS DOE DE-SCOO19186 and NSF-PHY 1725482 for access to the HERCULES laser facility. We also thank all of the staff of the Central Laser Facility and the Scientific Computing Department at UKRI-STFC Rutherford Appleton Laboratory. This work used the ARCHER2 UK National Supercomputing Service [43] and UKRI-STFCs SCARF cluster.

*Corresponding author.
marko.vonderleyen@physics.ox.ac.uk

[1] K. N. Kim, Y. Hwangbo, S.-g. Jeon, J. Kim, S. Han, and K. B. Kim, J. Korean Phys. Soc. **77**, 399 (2020).
[2] L. Labate, D. Palla, D. Panetta, F. Avella, F. Baffigi, F. Brandi, F. Di Martino, L. Fulgentini, A. Giulietti, P. Köster, D. Terzani, P. Tomassini, C. Traino, and L. A. Gizzi, Sci. Rep. **10**, 17307 (2020).
[3] M. Fuchs, R. Weingartner, A. Popp, Z. Major, S. Becker, J. Osterhoff, I. Cortrie, B. Zeitler, R. Hörlein, G. D. Tsakiris, U. Schramm, T. P. Rowlands-Rees, S. M. Hooker, D. Habs, F. Krausz, S. Karsch, and F. Grüner, Nat. Phys. **5**, 826 (2009).
[4] S. Kneip, C. McGuffey, F. Dollar, M. S. Bloom, V. Chvykov, G. Kalintchenko, K. Krushelnick, A. Maksimchuk, S. P. D. Mangles, T. Matsuoka, Z. Najmudin, C. A. J. Palmer, J. Schreiber, W. Schumaker, A. G. R. Thomas, and V. Yanovsky, Appl. Phys. Lett. **99**, 093701 (2011).
[5] J. M. Cole *et al.*, Proc. Natl. Acad. Sci. U.S.A. **115**, 6335 (2018).
[6] A. Döpp, L. Hehn, J. Götzfried, J. Wenz, M. Gilljohann, H. Ding, S. Schindler, F. Pfeiffer, and S. Karsch, Optica **5**, 199 (2018).
[7] T. Tajima and J. M. Dawson, Phys. Rev. Lett. **43**, 267 (1979).
[8] S. P. D. Mangles, C. D. Murphy, Z. Najmudin, A. G. R. Thomas, J. L. Collier, A. E. Dangor, E. J. Divall, P. S. Foster, J. G. Gallacher, C. J. Hooker, D. A. Jaroszynski, A. J. Langley, W. B. Mori, P. A. Norreys, F. S. Tsung, R. Viskup, B. R. Walton, and K. Krushelnick, Nature (London) **431**, 535 (2004).
[9] C. G. R. Geddes, C. Toth, J. van Tilborg, E. Esarey, C. B. Schroeder, D. Bruhwiler, C. Nieter, J. Cary, and W. P. Leemans, Nature (London) **431**, 538 (2004).
[10] J. Faure, Y. Glinec, A. Pukhov, S. Kiselev, S. Gordienko, E. Lefebvre, J.-P. Rousseau, F. Burgy, and V. Malka, Nature (London) **431**, 541 (2004).
[11] A. J. Gonsalves *et al.*, Phys. Rev. Lett. **122**, 084801 (2019).
[12] W. Lu, M. Tzoufras, C. Joshi, F. S. Tsung, W. B. Mori, J. Vieira, R. A. Fonseca, and L. O. Silva, Phys. Rev. ST Accel. Beams **10**, 061301 (2007).
[13] E. Esarey, C. B. Schroeder, and W. P. Leemans, Rev. Mod. Phys. **81**, 1229 (2009).
[14] S. Karsch, J. Osterhoff, A. Popp, T. P. Rowlands-Rees, Z. Major, M. Fuchs, B. Marx, R. Hrlein, K. Schmid, L. Veisz, S. Becker, U. Schramm, B. Hidding, G. Pretzler, D. Habs, F. Grner, F. Krausz, and S. M. Hooker, New J. Phys. **9**, 415 (2007).
[15] C. G. Durfee and H. M. Milchberg, Phys. Rev. Lett. **71**, 2409 (1993).
[16] Y. Ehrlich, C. Cohen, A. Zigler, J. Krall, P. Sprangle, and E. Esarey, Phys. Rev. Lett. **77**, 4186 (1996).

[17] D. J. Spence and S. M. Hooker, Phys. Rev. E **63**, 015401(R) (2000).
[18] R. J. Shalloo, C. Arran, L. Corner, J. Holloway, J. Jonnerby, R. Walczak, H. M. Milchberg, and S. M. Hooker, Phys. Rev. E **97**, 053203 (2018).
[19] A. Picksley, A. Alejo, J. Cowley, N. Bourgeois, L. Corner, L. Feder, J. Holloway, H. Jones, J. Jonnerby, H. M. Milchberg, L. R. Reid, A. J. Ross, R. Walczak, and S. M. Hooker, Phys. Rev. Accel. Beams **23**, 081303 (2020).
[20] P. Sprangle, C. Tang, and E. Esarey, IEEE Trans. Plasma Sci. **15**, 145 (1987).
[21] C. G. R. Geddes, K. Nakamura, G. R. Plateau, C. Toth, E. Cormier-Michel, E. Esarey, C. B. Schroeder, J. R. Cary, and W. P. Leemans, Phys. Rev. Lett. **100**, 215004 (2008).
[22] A. J. Gonsalves, K. Nakamura, C. Lin, D. Panasenko, S. Shiraishi, T. Sokollik, C. Benedetti, C. B. Schroeder, C. G. R. Geddes, J. van Tilborg, J. Osterhoff, E. Esarey, C. Toth, and W. P. Leemans, Nat. Phys. **7**, 862 (2011).
[23] K. Schmid, A. Buck, C. M. S. Sears, J. M. Mikhailova, R. Tautz, D. Herrmann, M. Geissler, F. Krausz, and L. Veisz, Phys. Rev. ST Accel. Beams **13**, 091301 (2010).
[24] A. Buck, J. Wenz, J. Xu, K. Khrennikov, K. Schmid, M. Heigoldt, J. M. Mikhailova, M. Geissler, B. Shen, F. Krausz, S. Karsch, and L. Veisz, Phys. Rev. Lett. **110**, 185006 (2013).
[25] L. T. Ke, K. Feng, W. T. Wang, Z. Y. Qin, C. H. Yu, Y. Wu, Y. Chen, R. Qi, Z. J. Zhang, Y. Xu, X. J. Yang, Y. X. Leng, J. S. Liu, R. X. Li, and Z. Z. Xu, Phys. Rev. Lett. **126**, 214801 (2021).
[26] C. McGuffey, A. G. R. Thomas, W. Schumaker, T. Matsuoka, V. Chvykov, F. J. Dollar, G. Kalintchenko, V. Yanovsky, A. Maksimchuk, K. Krushelnick, V. Y. Bychenkov, I. V. Glazyrin, and A. V. Karpeev, Phys. Rev. Lett. **104**, 025004 (2010).
[27] C. E. Clayton, J. E. Ralph, F. Albert, R. A. Fonseca, S. H. Glenzer, C. Joshi, W. Lu, K. A. Marsh, S. F. Martins, W. B. Mori, A. Pak, F. S. Tsung, B. B. Pollock, J. S. Ross, L. O. Silva, and D. H. Froula, Phys. Rev. Lett. **105**, 105003 (2010).
[28] M. Z. Mo, A. Ali, S. Fourmaux, P. Lassonde, J. C. Kieffer, and R. Fedosejevs, Appl. Phys. Lett. **100**, 074101 (2012).
[29] B. B. Pollock *et al.*, Phys. Rev. Lett. **107**, 045001 (2011).
[30] J. Faure, C. Rechatin, A. Norlin, A. Lifschitz, Y. Glinec, and V. Malka, Nature (London) **444**, 737 (2006).
[31] B. Hidding, G. Pretzler, J. B. Rosenzweig, T. Königstein, D. Schiller, and D. L. Bruhwiler, Phys. Rev. Lett. **108**, 035001 (2012).
[32] N. Bourgeois, J. Cowley, and S. M. Hooker, Phys. Rev. Lett. **111**, 155004 (2013).
[33] A. G. R. Thomas, C. D. Murphy, S. P. D. Mangles, A. E. Dangor, P. Foster, J. G. Gallacher, D. A. Jaroszynski, C. Kamperidis, K. L. Lancaster, P. A. Norreys, R. Viskup, K. Krushelnick, and Z. Najmudin, Phys. Rev. Lett. **100**, 255002 (2008).
[34] Y. Ma, D. Seipt, A. E. Hussein, S. Hakimi, N. F. Beier, S. B. Hansen, J. Hinojosa, A. Maksimchuk, J. Nees, K. Krushelnick, A. G. R. Thomas, and F. Dollar, Phys. Rev. Lett. **124**, 114801 (2020).
[35] L. Brieda, Particle push in magnetic field (boris method), https://www.particleincell.com/2011/vxb-rotation/ (accessed 22 May 2022).
[36] J. Boris, in *Proceedings of the Fourth Conference on Numerical Simulation of Plasmas* (United States Naval Research Office, Washington, 1970).
[37] C. Sheppard and T. Wilson, IEE J. Microw. Opt. Acoust. **2**, 105 (1978).
[38] S. V. Bulanov, F. Pegoraro, A. M. Pukhov, and A. S. Sakharov, Phys. Rev. Lett. **78**, 4205 (1997).
[39] A. G. R. Thomas, S. P. D. Mangles, Z. Najmudin, M. C. Kaluza, C. D. Murphy, and K. Krushelnick, Phys. Rev. Lett. **98**, 054802 (2007).
[40] S. Corde, C. Thaury, A. Lifschitz, G. Lambert, K. Ta Phuoc, X. Davoine, R. Lehe, D. Douillet, A. Rousse, and V. Malka, Nat. Commun. **4**, 1501 (2013).
[41] T. D. Arber, K. Bennett, C. S. Brady, A. Lawrence-Douglas, M. G. Ramsay, N. J. Sircombe, P. Gillies, R. G. Evans, H. Schmitz, A. R. Bell, and C. P. Ridgers, Plasma Phys. Control. Fusion **57**, 113001 (2015).
[42] S. M. Hooker, R. Bartolini, S. P. D. Mangles, A. Tnnermann, L. Corner, J. Limpert, A. Seryi, and R. Walczak, J. Phys. B **47**, 234003 (2014).
[43] http://www.archer2.ac.uk.